Science of the Total Environment 654 (2019) 1110–1117

Contents lists available at ScienceDirect

Science of the Total Environment

journal homepage: www.elsevier.com/locate/scitotenv

Fe^{2+} in ice cores as a new potential proxy to detect past volcanic eruptions

François Burgay [a,*], Tobias Erhardt [b], Damiano Della Lunga [c], Camilla Marie Jensen [b], Andrea Spolaor [d], Paul Vallelonga [e], Hubertus Fischer [b], Carlo Barbante [a,d]

[a] Department on Environmental Science, Informatics and Statistics, Ca' Foscari, University of Venice, Venice, Italy
[b] Climate and Environmental Physics, Physics Institute and Oeschger Centre for Climate Change Research, University of Bern, Bern, Switzerland
[c] Alfred Wegener Institute, Helmholtz-Zentrum fur Polar und Meeresforschung, Bremerhaven, Germany
[d] National Research Council, Institute for the Dynamics of Environmental Processes, Venice, Italy
[e] Centre for Ice and Climate, Niels Bohr Institute, University of Copenhagen, Copenhagen K, Denmark

HIGHLIGHTS

- Development of a new method for Fe^{2+} quantification in ice cores
- High Fe^{2+} concentrations in coincidence with volcanic eruptions
- Fe^{2+} as a new potential proxy to identify past volcanic eruptions

GRAPHICAL ABSTRACT

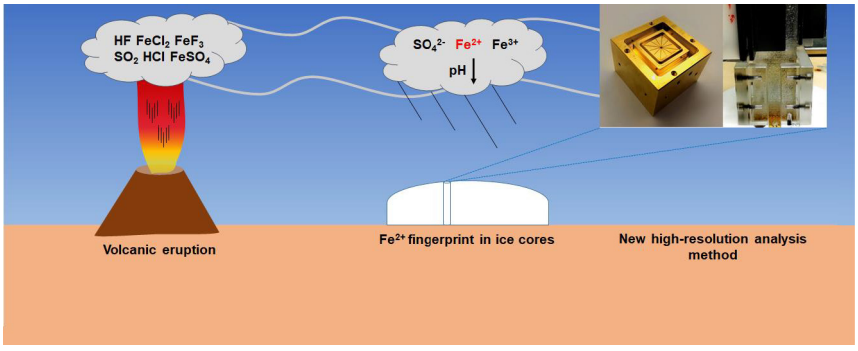

ARTICLE INFO

Article history:
Received 24 July 2018
Received in revised form 5 November 2018
Accepted 6 November 2018
Available online 07 November 2018

Editor: Mae Sexauer Gustin

Keywords:
Iron speciation
Volcano
Continuous flow analysis
Chemiluminescence
Greenland

ABSTRACT

Volcanic eruptions are widely used in ice core science to date or synchronize ice cores. Volcanoes emit large amounts of SO_2 that is subsequently converted in the atmosphere into sulfuric acid/sulphate. Its discrete and continuous quantification is currently used to determine the ice layers impacted by volcanic emissions, but available high-resolution sulphate quantification methods in ice core (Continuous Flow Analysis (CFA)) struggle with insufficient sensitivity. Here, we present a new high-resolution CFA chemiluminescence method for the continuous determination of Fe^{2+} species in ice cores that shows clear Fe^{2+} peaks concurrent with volcanic sulphate peaks in the ice core record. The method, applied on a Greenland ice core, correctly identifies all volcanic eruptions from between 1588 to 1611 and from 1777 to 1850. The method has a detection limit of ~5 pg g^{-1} and a quadratic polynomial calibration range of up to at least 1760 pg g^{-1}. Our results show that Fe^{2+} is a suitable proxy for identifying past volcanic events.

1. Introduction

Explosive volcanic eruptions have the potential to cool the Earth and affect the climate on annual to multiannual time scales through the injection of large quantities of gases and fine particles both into the

* Corresponding author.
E-mail address: francois.burgay@unive.it (F. Burgay).

https://doi.org/10.1016/j.scitotenv.2018.11.075
0048-9697/

troposphere and in the stratosphere (Oppenheimer, 2003). This can lead to a global increase in the Earth's albedo resulting in a decrease in average surface temperatures. To define the magnitude of a volcanic eruption, the Volcanic Explosivity Index (VEI) is commonly used (Newhall and Self, 1982). The VEI classifies volcanic eruptions through the volume of erupted tephra and the eruption column height. Its values range from 0 (Hawaiian eruption) to 8 (Ultra-Plinian eruption). It has been reported that explosive eruptions (VEI > 6) have the capacity to cool the Earth's climate from between 0.2 °C to 2.7 °C for several years (Sigl et al., 2015; Zielinski, 2000). Although explosivity as indicated by the VEI and volcanic sulphur injection into the stratosphere do not necessarily follow a one-to-one relationship. Ultra-Plinian eruptions, such as the Toba eruption (≈73 kya), could have affected the climate on a centennial time scale and could have even been involved in glaciation/deglaciation processes (Huybers and Langmuir, 2009; Williams, 2012).

Besides being an important source of sulphate aerosol, Spirakis (1991) first suggested that volcanoes could be a significant source of bioavailable Fe, potentially triggering phytoplankton blooms in the so-called High Nutrient Low Chlorophyll (HNLC) regions. HNLC areas (e.g. the Southern Ocean or the North East Pacific) are oceanic regions where Marine Primary Productivity (MPP), as reflected in the production of chlorophyll, is very low although macronutrient concentration (mainly NO_3^-) is high. In these areas, productivity is controlled by the availability of micronutrients, such as iron (Martin and Fitzwater, 1988; Martin et al., 1990). Volcanic ash typically contains highly soluble iron salts such as $FeCl_2$, $FeCl_3$, FeF_2, FeF_3 and $FeSO_4 \cdot 7H_2O$ (Langmann et al., 2010) and 10^{10} g or more of Fe can be released into the ocean, depending on the magnitude of the volcanic eruption (Watson, 1997).

Because of their important climatic relevance, identifying and dating volcanic events is crucial to quantify and better assess their impact on climate (Sigl et al., 2013). Ice cores provide a continuous high-resolution archive to reconstruct the volcanic fingerprint on the Earth system and volcanic horizons are used, together with other proxies, to date and synchronize cores (Vinther et al., 2006). Up to now, volcanic eruptions have been identified in ice cores through pH measurements or through SO_4^{2-} and elemental sulphur quantification. pH is commonly quantified through an absorption method (Kjær et al., 2016), while sulphates are determined by: ion chromatography (Gautier et al., 2015), fast chromatography (Severi et al., 2015) and continuous flow analysis (CFA) using methylthymol blue (Bigler et al., 2002; Madsen and Murphy, 1981; Röthlisberger et al., 2000). High-resolution measurements of sulphur are also routinely performed by Inductively Coupled Plasma Mass Spectrometer (ICP-MS) (Sigl et al., 2014; Sigl et al., 2015). Besides these approaches, studies performed on ice cores collected in Greenland (Spolaor et al., 2013b) and in Antarctica (Spolaor et al., 2013a; Spolaor et al., 2012) showed that peaks both in soluble iron and Fe^{2+} were associated to volcanic events suggesting that they might be promising proxies to detect past volcanic eruptions.

Considering that Fe^{2+} species are very reactive and they quickly oxidize when in contact with air, their quantification is not straightforward. Several methods exist to quantify Fe^{2+} in seawater (Achterberg et al., 2001; Hansard and Landing, 2009), sea-ice (Lannuzel et al., 2006) and ice cores (Spolaor et al., 2013a; Spolaor et al., 2012; Spolaor et al., 2013b). We can classify them into three categories: 1) absorption spectrometry (Spolaor et al., 2013a; Spolaor et al., 2012); 2) Spectrophotometric techniques (Chan et al., 2016; Majestic et al., 2006; Pullin and Cabaniss, 2001; Stookey, 1970) and 3) chemiluminescence (CL) techniques (Schallenberg et al., 2016). For polar ice core analysis, the method proposed by Spolaor et al. (2012, 2013a) struggled to achieve the required high-resolution and the Limit of Detection (LoD). Thus, considering the detection limits of the above-mentioned approaches and the concentrations of Fe^{2+} in ice and snow (ranging from <1 pg g^{-1} up to 1 ng g^{-1}) (Spolaor et al., 2012), CL guarantees the lowest LoD, the highest response and the lowest memory effects when linked to CFA (Table S1).

This work presents the first application of a chemiluminescence method coupled to a continuous flow analysis system (CFA-CL-Fe^{2+}) for the determination of Fe^{2+} species in ice cores. The method was applied for the analysis of a firn-ice core from North Greenland (B17), to detect the main volcanic events from 1588 to 1850. For this purpose, a comparison with discrete SO_4^{2-} analyses was performed as well. Additionally, an improved version of the absorption Fe_{tot} method (Hiscock et al., 2013; Spolaor et al., 2013b) was tested on the B17 ice core. Finally, merging these data with the total iron measurements collected using inductively coupled plasma time of flight mass spectrometry (ICP-TOF) analysis, we present the first complete continuous iron chemical speciation dataset ever to be retrieved from an ice core.

2. Material and methods

2.1. Sample preparation, analysed sections and dating

The 100.8 m deep B17 ice core was drilled within the framework of the North Greenland Traverse (NGT) in 1993 at 2820 m a.s.l. (75.25°N; 37.63°W), east of the main ice divide. The ice core was dated using volcanic horizons resulting in a maximum core age of 1363 CE, meaning the site had an average accumulation rate of 114 $kg \cdot m^{-2} \cdot yr^{-1}$ (Weissbach et al., 2016). The analysed sections, the melt speed and chronology are reported in Table S2.

2.2. Iron (II)

The CL induced by the reaction between luminol, O_2 and Fe^{2+} is widely used in oceanography (Hansard and Landing, 2009; Rose and Waite, 2001; Santana-González et al., 2017; Schallenberg et al., 2016) and has been used to analyse sea-ice (Lannuzel et al., 2006), it has a low detection limit (<10 pg g^{-1}), high sensitivity and no memory effects. The sensitivity of the method depends on the pH at which the luminol solution is buffered. Seitz and Hercules (Seitz and Hercules, 1972), found that at pH = 10.3 the sensitivity was the highest and the reaction between Fe^{2+} species and the oxygen dissolved in the reagent is most favourable. This reaction leads to the production of superoxide radicals that in turn oxidize luminol to the excited α-hydroxy-hydroperoxide (α-HHP) species. It is the decomposition of the α-HHP that results in a blue light emission at $\lambda_{max} = 425$ nm. The recorded signal is proportional to the concentration of Fe^{2+} in the sample. Different authors reported either linear (Croot and Laan, 2002; Hansard and Landing, 2009) or polynomial (King et al., 1995; Rose and Waite, 2001) calibration curves. This depends on both the sample matrix and on the concentration range used in the calibration.

Luminol has some interferences. Studies (Lannuzel et al., 2006) conducted after spiking Antarctic seawater with a nominal concentration of 2 nM Fe^{2+} with Co(II), Mn(II), Cu(II), Zn(II), Cr(III), Cd(II) and Ni(II) showed interference effects with Cu(II). This is was due to Cu(II) participating in the redox reaction with Fe^{2+} resulting in signal suppression (González et al., 2016). The other interferent was Co(II) which can result in an overestimation of the signal if the concentration was more than two times higher than Fe^{2+} (Lannuzel et al., 2006). The concentrations levels in Greenland ice core of these two interferents are comparable to or below the concentrations of Fe^{2+}, meaning it is unlikely that they could interfere during the analysis of our sample. For instance, Cobalt concentration in the Summit ice core (Greenland) ranged from 0.65 pg g^{-1} to 15.5 pg g^{-1} (with an average value of 5.8 pg g^{-1}) (Barbante et al., 1997).

2.2.1. Fe(II) - reagents and standards

All the plastic material used for analyses was cleaned following the procedure illustrated in the Supplementary material (S1).

The reagents were prepared as follows:

- *Fe(II) carrier:* HCl 0.001 M was prepared diluting 50 μl of the 37% HCl (ACS reagent, Sigma Aldrich, USA) in 500 ml Ultra Pure Water (UPW) water.
- *Luminol solution:* dissolution of 0.178 g of Luminol (Sigma Aldrich, USA) in 1 M NH_3 solution (73 ml of Ammonium Hydroxide Solution (TraceSELECT™, Honeywell Fluka, USA) in 1 L of UWP water). The solution was stirred for 60 s and then stored for 12/24 h to ensure complete dissolution. After that, the pH was adjusted to 10.3 with the addition of 10–15 ml of HCl (ACS reagent, Sigma Aldrich, USA). To enhance sensitivity, the solution was ultrasonicated for 30′ and then cooled to room temperature. Because luminol is light-sensitive (Rose and Waite, 2001), the solution was stored in dark HDPE bottles and all tubing was shielded from light. The luminol solution was prepared at least 2 days before the analytical session, in order to be sure that it was all in the dissolved form.
- *Fe(II) standards:* a standard stock solution was prepared by dissolving 0.3921 g of ammonium iron (II) sulphate hexahydrate (Honeywell Fluka, USA) in a 100 ml 0.1 M HCl solution. Even if the solution is stable up to one month (Hansard and Landing, 2009), we prepared it every week. One intermediate (50 μM) and one working solution (250 nM) were prepared daily by dilution of the stock solution and acidified with 300 μl HCL 37% (ACS reagent, Sigma Aldrich, USA). The calibration was made with the standard addition method with standards prepared fresh every 2 h.

2.2.2. Fe(II) – instrumental setup

Tygon pump tubing and 1/16″ PTFE Tubing and high-pressure fittings are used to carry reagents and samples to the detectors via an 8-channel peristaltic pump (Ismatec, Germany) at a rate of 27 rpm. Flow rates and the length of PTFE Tubing are optimized to minimize backpressure issues (Fig. 1). For the luminol detection, we used a custom-made spiral flow cell made by a 25 cm PTFE Tubing (1/16″, 0.75 mm ID, VICI, USA) put in front of a photomultiplier (SensTech, USA) completely shielded from light. All data were acquired every second using the Sens-Tech Counter Timer 2.8 software (Sens-Tech Ltd., USA).

2.3. Total soluble iron method

The total soluble iron method relies on the catalytic oxidation of the *N*,*N*-Dimethyl-*p*-phenylenediamine dihydrochloride (DPD) to the semiquinonic form (DPDQ) driven by Fe(III) species (Hiscock et al., 2013; Spolaor et al., 2013b). Hydrogen peroxide is added to the sample to oxidize both the Fe^{2+} originally present in the sample and the one that is formed after the reduction of Fe^{3+} when it reacts with the DPD (Traversi et al., 2004). The quantification of total soluble iron is possible by monitoring absorption at 514 nm where DPDQ shows an absorption maximum (Yuan and Resing, 1995).

Details of reagent and standard preparation (S2), instrumental setup (S3) and its optimization (S4) are reported in the supplementary information. The instrumental setup is shown in Fig. 1.

2.4. Coupling with the CFA-system

Both the Fe^{2+} and total soluble iron method were developed in the laboratories of the Ca' Foscari University of Venice and the Institute for the Dynamic of Environmental Processes of the National Research Council (IDPA-CNR). Both methods were coupled with the Bern CFA system used for ice core analysis, which routinely measures dust (Abakus Klotz, Germany), conductivity (Amber Science, USA) and major ions such as Na^+, Ca^{2+}, NH_4^+, NO_3^-, and H_2O_2 with different spectrophotometric techniques (based on absorption or fluorescence) (Kaufmann et al., 2008). The system also has a stream that sends melted ice core samples to an Inductively Coupled Plasma Time of Flight Mass Spectrometer (ICP-TOF-MS) and to an autosampler for discrete anions measurements. The melting unit is located into a freezer (Temp = −20 °C) where ice cores are processed and cut (cross section 34 × 34 mm). All the instruments are located in a normal laboratory and thermostatically-controlled at +20 °C.

The temperature of the melthead was regulated to control the melting speed, which can vary from 3.4 cm min^{-1} to 3.2 cm min^{-1} for the upper lower density firn layers (down to a depth of about 45 m) to <2.5 cm min^{-1} for the deepest part (down to 70.0 m). Details about the melt speeds are provided in Table S2.

2.5. Total iron determination by ICP-TOF-MS

Total iron concentrations were measured using an ICP-TOF-MS (icpTOF, Tofwerk, Thun, Switzerland) (Hendriks et al., 2017) directly connected to the meltwater stream of the Bern CFA system (Erhardt et al. in prep). Similar to other CFA-ICP-MS setups (Knüsel et al., 2003; McConnell et al., 2002), the sample stream was acidified on-line to 1% HNO_3 (Optima grade, Fisher, USA) adding an internal standard, in this case Rh (TraceCert, Sigma Aldrich, USA), to assess system stability. The system uses a glass concentric nebulizer (Glass Expansion, Australia) and peltier-cooled cyclonic spay chamber.

To enable the determination of iron using ^{56}Fe, the collision/reaction cell (Q-Cell) of the icpTOF was pressurized with a mixture of 7% H_2 and 93% He at a flow rate of 5 ml/min.

Calibration measurements where performed before and after each measurement run using dilutions of multi-element standard solution (TraceCert, Sigma Aldrich) ranging from 2 to 20 ng g^{-1}.

Data acquisition was run at 250 ms integration time and the data was subsequently down-sampled to 1 mm nominal depth resolution.

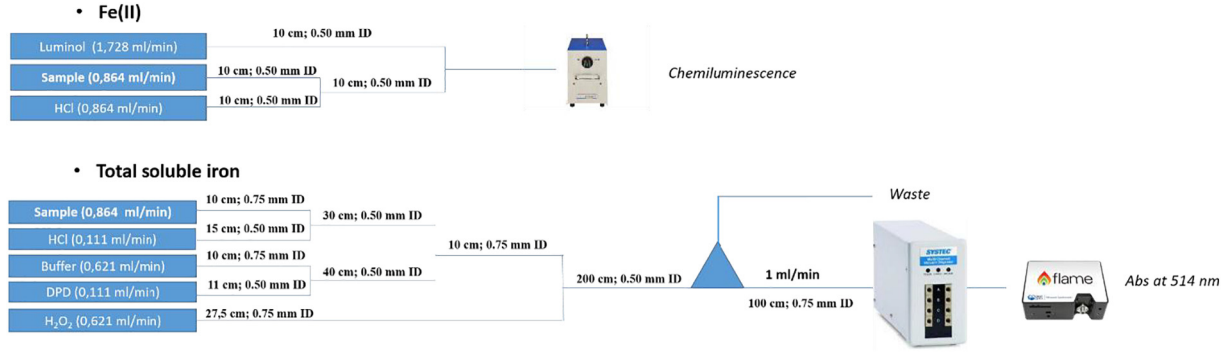

Fig. 1. Analytical setup with optimized flow and tubing length according with the Hagen-Poiseuille law.

Average sensitivities for total iron were 11 kcps·ng·g^{-1} at <1.5% RSD and detection limits of 0.13 ng g^{-1} at 250 ms integration time resulting in a LoD of 0.043 ng g^{-1} for the 1 mm resolution data reported here.

2.6. Discrete sulphate determination

Sulphate measurements were performed on discrete samples collected at a nominal resolution of 2 to 5 cm and later analysed at the Alfred Wegener Institute in Bremerhaven by Ion Chromatography (Dionex 5000+, ThermoFisher Scientific, USA). Details about the LoD and the capillary column are reported in the Supplementary material (S5).

3. Results

3.1. Iron (II)

3.1.1. Calibration and matrix effects

Possible matrix effects have been investigated using two melted ice samples, aged >48 h and stored in dark conditions at +4 °C to ensure the full oxidation of the Fe^{2+} in the matrix. The slope of the external calibration obtained with real Antarctic melted ice (black line, Fig. 2) was compared with the calibration curve prepared in Ultra-Pure Water (UPW, red line, Fig. 2). The sensitivity in UPW was 272,178 $(ng\ g^{-1})^{-1}$, compared to 95,579 $(ng\ g^{-1})^{-1}$ for standards prepared in a melted Antarctic ice matrix. Our findings are in line with results found in seawater samples (Hansard and Landing, 2009), freshwater samples (Emmenegger et al., 1998), sea-ice samples (Lannuzel et al., 2006) and other matrices (Saitoh et al., 1998).

To correct for matrix effects, uncontaminated outflow from the melter unit was collected and stored in the dark at +4 °C for 48 h, to ensure oxidation of all the Fe^{2+} on the sample (Hansard and Landing, 2009). Considering that the main Fe^{2+} interferons (Cu and Co) in oxic environments are mainly present in their Cu(II) and Co(II) oxidation states (Collins and Kinsela, 2010), which are also the most thermodynamically stable, the Fe^{2+} subsequently spiked to the aged matrix, will experience the same "matrix effect" also after 48 h of storing. Acidity might also lead to an increase in the analytical signal (Hansard and Landing, 2009). We found from other discrete ice core analyses that acidifying a melted ice core sample to pH = 2 significantly increased the signal. This is the reason why, during the set-up of this continuous analytical method we decided to acidify the sample inline and before the luminol detection. In particular, the pH of the sample (normally around 5.6; Kjær et al., 2016) is brought to pH = 3.30 when mixed with the HCl carrier at pH = 3. Typical pH values for ice with volcanic eruptions are around 4.0–4.5 (Kjær et al., 2016). This means that, when these events occurred, the pH of the sample after its mixing with the carrier, is brought to pH = 3.26 (ΔpH = 0.04). Considering also the buffering potential of the luminol solution, we concluded that the method is not affected by the pH changes that might occur during volcanic events.

Standard addition of 55 pg g^{-1}, 110 pg g^{-1} and 220 pg g^{-1} of Fe^{2+} were added to the melted ice matrix to create a matrix matched calibration curve. The dynamic range was determined by adding standards with concentrations from 55 pg g^{-1} to 1760 pg·g^{-1} to an aged B17 ice matrix sample (Fig. 3). The obtained calibration curve was polynomial ($R^2 \geq 0.99$) demonstrating the reliability of this calibration method for quantifying Fe^{2+} in ice cores.

3.1.2. Accuracy, reproducibility and Limit of Detection (LoD)

To define the accuracy of the method, a certificate material is needed. Unfortunately, no Fe^{2+} certified material exists for ice matrices. This is the reason why we quantified the accuracy by carrying out recovery tests. A calibration curve was realized using two ice core matrices: Dome C from Antarctica and NEEM from Greenland. These matrices were spiked with known concentration of Fe^{2+} (55 pg g^{-1}, 275 pg g^{-1} and 550 pg g^{-1}). Subsequently, we added to the same aged Dome C and NEEM matrices, 220 pg g^{-1} and 110 pg g^{-1} of Fe^{2+}

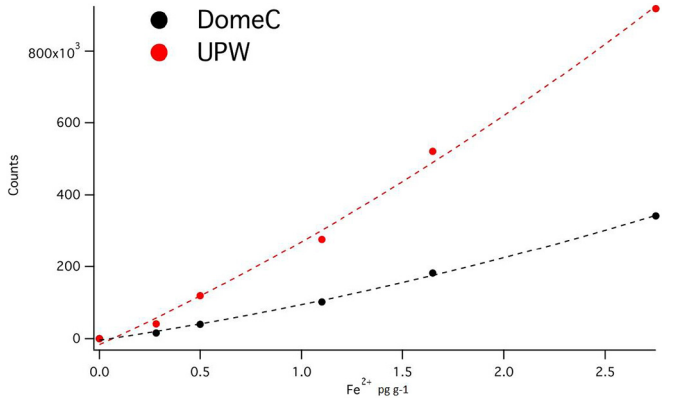

Fig. 2. Different matrices result in different calibration curves. In red, standards prepared in MQ water, in black standards prepared with standard additions from a Dome C matrix. (For interpretation of the references to color in this figure legend, the reader is referred to the web version of this article.)

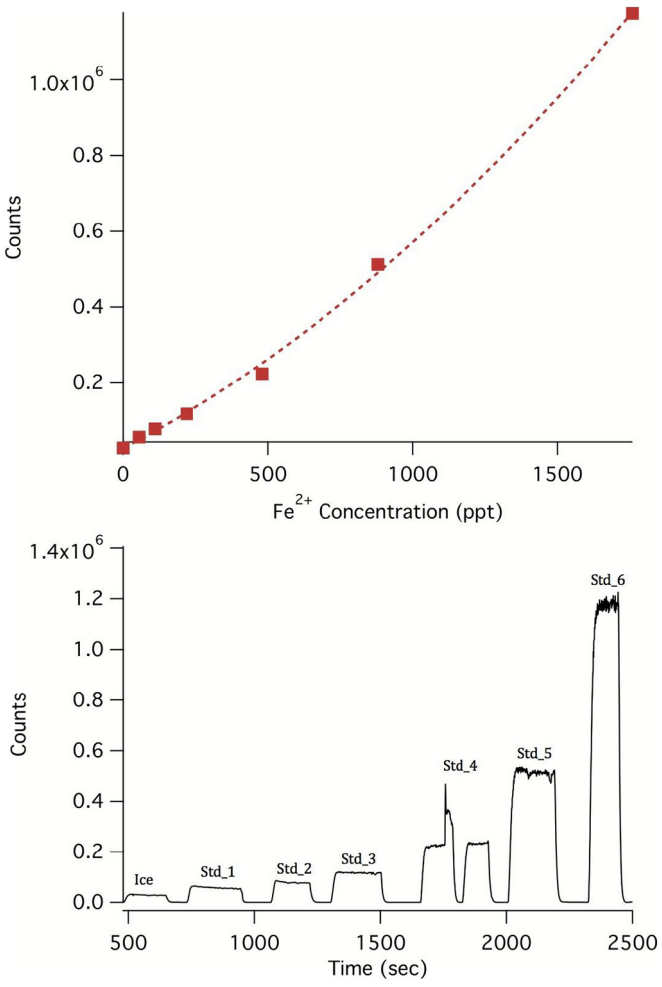

Fig. 3. Calibration curve ($y = 0.1467x^2 + 395.57x$; $R^2 = 0.9988$) from 55 pg g^{-1} to 1760 pg g^{-1}, to evaluate the dynamic range performed on the aged B17 matrix.

respectively. The recovery was found to be 99.4% for Dome C (218 ± 4 pg g^{-1}) and 113% for NEEM (124 ± 3 pg g^{-1}).

To estimate the reproducibility, we carried out four measurements of three different standards during the analytical run (Table S3). Each standard was prepared fresh before each measurement to avoid oxidation problems. Because of the Fe^{2+} oxidation kinetic, we did not read the same sample for four times. According with the kinetic tests we performed on a real B17 matrix and considering that four readings of the same sample might take up to 5–10 min, the Fe^{2+} loss can be >5%, leading to an underestimation of the actual reproducibility. The measurement lasted 60 s with a 1-s integration time. The reported value is the averaged one. We conclude that reproducibility of the method is within the range of 3–4% RSD.

The detection limit was calculated by repeated analysis of the matrix after storage for 48 h in the dark at +4 °C. The LoD was calculated as three times the standard deviation of the blank concentration. It was found to vary between 0.5 pg g^{-1} to 10 pg g^{-1} (mean value: 4.5 pg g^{-1}). Comparison of these results with the ICP-MS method (Spolaor et al., 2012) shows that the luminol method is an order of magnitude more sensitive.

3.1.3. Sensitivity

According to literature studies, calibration curves are reported to be either linear (Hansard and Landing, 2009) or second order polynomial (Croot and Laan, 2002; Lannuzel et al., 2006; Rose and Waite, 2001). During the analytical session, we calibrated our data using either linear or polynomial curve fitting. The observation of different calibration curves, as reported by Rose and Waite in their review (Rose and Waite, 2001), is due to the variability of the boundary conditions (temperature, light conditions, impurities…) from one day to the other. In particular, light and some impurities present in the reagents may lead to the production of free radicals during the analysis, changing the sensitivity of the method (Rose and Waite, 2001). As an example, we report how our calibration changed during an analytical session on 1 day (Table S4) and, with it, the sensitivity. The obtained sensitivity was significantly lower than the one obtained for the Antarctic matrix. This is mainly attributable to the fact that the reagents are prepared daily and slight differences in the analytical conditions (e.g. light, impurities in the reagents…) might occur.

The sensitivity for the polynomial calibration was obtained by calculating the first derivative of the calibration curve at the point x_0, where $x_0 = 110$ pg g^{-1}.

We performed a calibration with freshly prepared standards every three or four runs, which means approximately every 2 h. For our studies, we used a polynomial fit only when the R^2 for the linear one was <0.99. However, it is worth noting that during the same day we used either polynomial or linear fittings for all the calibrations. This suggests that the "day by day" different conditions (especially in terms of reagent preparation, shielding of tubing…) caused the observed differences in terms of calibration fitting. We did not observe significant changes in the sensitivity from the upper part of the core to the lowest part of the core mainly because of the limited time frame that we analysed. However, further investigations are suggested on deeper ice cores.

3.1.4. Fe^{2+} oxidation in melted ice matrices

The target Fe^{2+} species are easily oxidized by O_2 to the more stable Fe^{3+} species. To understand the kinetics of this in ice matrices, we followed the oxidation of 55 pg g^{-1} of Fe^{2+} added to an aged ice matrix from B17 at room temperature or unacidified UPW.

The Fe^{2+} oxidation follows a first order kinetics but it is fastest in the B17 matrix (Fig. S1). In particular, Fe^{2+} in B17 (blue dots, Fig. S1) has a shorter half-life (117 min) than that in UPW (347 min, yellow dots, Fig. S1).

Our findings, summarised in Table S2 were compared with the results obtained by Spolaor et al., 2013a. This study reports a half-life for the Fe^{2+} oxidation in acidified UWP in the order of 250 min. Our results together with data reported in literature (Morgan and Lahav, 2007; Spolaor et al., 2013a; Zhuang et al., 1995) suggest that there will not be a significant Fe^{2+} loss (<1%) during transfer from the melt head to the detector (transfer time, approximately 90 s).

3.1.5. Comparison between the continuous Fe^{2+} and the continuous SO_4^{2-} determination

Up to now, SO_4^{2-} has been indirectly quantified through the competitive reactions between SO_4^{2-} and Ba^{2+}, and between Ba^{2+} and methylthymol blue (MTB). Thus, the quantification of sulphate is possible by either monitoring the absorbance at 460 nm for the uncomplexed MTB or at 608 nm for the MTB-barium complex (Bigler et al., 2002). As sulphate concentration increases, the concentration of MTB-Ba decreases while the concentration of the uncomplexed MTB increases. In this section, we want to compare the analytical performance of this method with the sensitivity of the new Fe^{2+} approach. Starting from the simpler analytical setup, we show that Fe^{2+} is a suitable alternative to detecting volcanic eruptions.

If we compare the method performances between the two CFA methods (Table 1) focusing on the Huaynaputina (1600 CE) eruption, we observe that the CFA-CL-Fe^{2+} method shows a higher signal to noise (S/N) ratio (S/N = 45) than the sulphate method (S/N = 10) (Bigler et al., 2002). Furthermore, the CFA-CL-Fe^{2+} method has a LoD that is 5 orders of magnitude lower than the sulphate MTB method we reported. The results suggest that this new approach has the sensitivity needed to detect even less intense volcanic eruptions.

3.2. Total soluble iron

3.2.1. Accuracy, reproducibility and LoD

For the total soluble iron method, we tested the accuracy with a spike recovery test. A standard of known concentration (0.50 ng g^{-1}) prepared in UPW was analysed against a calibration curve (from 0.047 ng g^{-1} to 1 ng g^{-1}, $R^2 = 0.99$). The concentration found (0.52 ± 0.04) ng g^{-1} corresponds to a spike recovery of 96%.

Reproducibility was tested with 5 replicate measurements of 0.5 ng g^{-1} and 1 ng g^{-1} standards. With a 6000 μs integration times, we found the precision was between 2 and 7% RSD. Precision was worse for lower standards: for a standard at 0.05 ng g^{-1}, it was found to be 19% RSD, suggesting we were approaching the LoD.

The LoD was 0.020 ng·g^{-1}, lower than that reported by both Traversi et al. (2004) and Spolaor et al. (2013b) but of the same order of magnitude as the one obtained by Hiscock et al. (2013).

3.2.2. Matrix effects

The absorption method to detect total soluble iron relies on the catalytic reaction of Fe(III) on the oxidation of *N*,*N*-dimethyl-*p*-phenylenediamine by hydrogen peroxide in weakly acidic media to a semiquinonic form (Hirayama and Unohara, 1988). Absorption was monitored at 514 nm. It was applied successfully to ice cores analysis with detection limits lower than 0.05 ng g^{-1} (Hiscock et al., 2013; Spolaor et al., 2013b; Traversi et al., 2004).

For the analysis of the B17 ice core, we optimized the method and we investigated the matrix effects. To our knowledge, no studies have been performed before on possible matrix effects of the total soluble iron method in ice samples. We performed an external calibration and a standard addition calibration and we compared the slope of the resulting calibration curves. The slopes of both curves were not significantly different, meaning that the total soluble iron method does not show any appreciable matrix effects in ice.

3.2.3. Calibration and sensitivity

Regular calibrations were done every three or four runs (after approximately 2 h) with a linear calibration curve having a $R^2 > 0.99$ in the range 0.5 ng g^{-1}, 1.0 ng g^{-1}, 1.5 ng g^{-1} (Table S6).

Table 1
Comparison among the Fe(II)-CL and the available SO_4^{2-} method performances. S/N ratio are evaluated for 200 ng·g^{-1} (sulphate method) and 300 pg·g^{-1} for the Fe(II) method.

	LOD	Sensitivity	Accuracy	Precision	S/N ratio	Matrix effect
Fe^{2+} method (This work)	4.5 pg·g^{-1}	1750 (pg g^{-1})$^{-1}$	99–113%	3–4%	45	Yes
SO_4^{2-} method (Bigler et al., 2002)	40 ng·g^{-1}	0.25 (ng g^{-1})$^{-1}$	67–99%	15%	10	No

We performed a linearity test from 0.5 ng g^{-1} to 8 ng g^{-1}. We found that the method is linear up to the highest standard ($R^2 = 0.99$) and with no memory effect. This result agrees with previous findings (Hiscock et al., 2013; Spolaor et al., 2013b; Traversi et al., 2004) providing a reliable quantification of the total dissolved iron in Greenland ice.

3.3. Iron species in the B17 ice core

With the new CFA-CL-Fe^{2+} method, the optimized total soluble iron method and the total iron method were applied to selected sections of the B17 ice core: from 1777 CE to 1850 CE (Fig. 4, left panel) and from 1589 CE to 1611 CE (Fig. 4, right panel). Values for total soluble iron vary from the LoD (0.020 ng g^{-1}) to 4 ng g^{-1}, while Fe^{2+} concentration ranged from the LoD (0.0045 ng g^{-1}) up to 590 pg g^{-1}. Total iron values ranged from the LoD (0.043 ng g^{-1}) to 25 ng g^{-1}.

Both total soluble iron and total iron show a seasonal pattern corresponding to the winter/spring maximum in dust fluxes (Lupker et al., 2010), while the Fe^{2+} signal is mainly influenced by volcanic events where it can be up to 50 times higher than the baseline.

Time series of conductivity, dust and sulphate are also included.

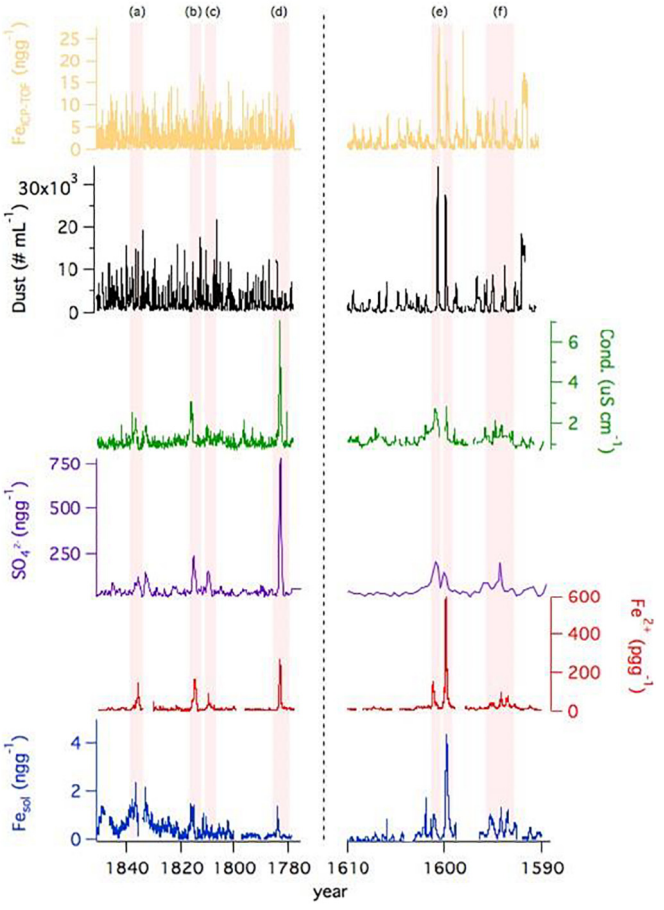

Fig. 4. Total iron, dust, conductivity, discrete sulphate, Fe^{2+} and total soluble iron from the B17 ice core. In the shadowed area we highlight the main eruptions detected in the ice core. In particular: a) Cosiguina, 1836; b) Tambora, 1815; c) Unkown 1810; d) Laki, 1783; e) Huaynaputina, 1600 (the double peak refers to the same eruption, see text for further details); f) Ruiz, 1596 and Raung, 1594.

4. Discussion

Owing to the new CFA-CL-Fe^{2+} method, we have acquired both total iron and total soluble iron simultaneously in continuous mode and, together with dust and conductivity, we identified several volcanic eruptions throughout the B17 ice core. The matching of sulphate and Fe^{2+} suggested that the new CL-based method could be used as a reliable proxy for past volcanic eruptions. Some data associated to Fe^{2+} and soluble Fe are missing because we experienced troubles with air bubbles and we stopped the data acquisition for these specific sections.

4.1. Fe^{2+} as a proxy for past volcanic eruptions

Performing an outliner method detection (S6) a high correspondence between sulphate in discrete samples, the main proxy for detecting past volcanic eruptions, and our Fe^{2+} data was found. In particular, the 86% of the SO_4^{2-} peaks were associated to Fe^{2+} peaks. Only one eruption, the Ruiz (1596 CE), did not result into a significant sulphate outliner and this can be explained by the low VEI that this eruption has. Thanks to the available ice core dating (Weissbach et al., 2016), we were able to associate Fe^{2+} peaks to specific volcanic eruptions (Table 2). We performed continuous iron analysis from 1850 to 1777 and from 1611 to 1589 where we expected to find the most intense volcanic eruptions.

In the first time window (Fig. 4, left panel) we associated the signal detected in 1836 to the Cosigüina eruption (12.98°N, 87.34°W) (Longpré et al., 2014). The eruption of Volcán Cosigüina was one of the largest and most explosive in Central America since Spanish colonization (Scott et al., 2006) with a global stratospheric sulphate aerosol injection of 40.2 Tg and 13.4 Tg of sulphur (Longpré et al., 2014). We also detected the Tambora eruption in 1816 (8.15°S 118.00°E). The Tambora eruption in Indonesia has been recognized as the largest known historic eruption with 140 Gt of expelled magma and with 60 Megaton (Mt) of sulphur injected into the stratosphere, six times more than the 1991 Pinatubo eruption. This led to a pronounced cooling of approximately 0.4–0.8 °C relative to the preceding 30 years (D'Arrigo et al., 2009) of temperature in Europe. The radiative forcing produced by Tambora in the year that followed the eruption was about −5 W·m^{-2} (Raible et al., 2016). This phenomenon was also known as the "year without summer" (Oppenheimer, 2003). According to other ice core measurements (Yalcin et al., 2006), we have also detected the eruption of an unknown tropical volcano at around 1810 (Dai et al., 1991). The Laki eruption in 1783–1785 is recognizable as well. This eruption emitted approximately 122 Mt SO_2 into the atmosphere and led to an unusual hot summer followed by a severe winter in Europe and North America with an annual mean surface cooling of about 1.3 °C which lasted for 2–3 years (Thordarson and Self, 2003).

In the other considered time window (Fig. 4, right panel), we found the Huaynaputina (16°36′30″S 70°51′00″W) eruption in 1600. Thanks to the high resolution profile, we detected two different peaks suggesting that the eruption could have occurred over two different periods. From 1594 to 1596 we detected an increase in sulphate and soluble Fe concentrations. It is difficult to associate these events to a precise

Table 2
Main eruptions identified through the new approach. n.a. = not available. Distance is reported as direct line (as the crow flies) from the volcano to the B17 site. The VEI values are provided by the NOAA volcano database available online National Geophysical Data Center/World Data Service (NGDC/WDS): Significant Volcanic Eruptions Database. National Geophysical Data Center, NOAA. doi:https://doi.org/10.7289/V5JW8BSH.

Year	Volcanic event	VEI	Distance/km	$[Fe^{2+}]$ /pg g^{-1}	[Soluble Fe] /ng g^{-1}	[Total Fe] /ng g^{-1}	$[Fe^{2+}]$/ [soluble Fe]	[Soluble Fe] /[total Fe]	$[SO_4^{2-}]$ /ng g^{-1}
1836	Cosigüina	5	7500	150	2.0	4.0	0.08	0.5	110
1816	Tambora	7	12,400	160	1.4	3.7	0.11	0.4	217
1810	Unknown	≥5	n.a.	90	0.9	5	0.10	0.2	130
1783	Laki	6	1400	260	1.3	6.3	0.20	0.2	780
1600	Huaynaputina	6	10,500	570	4.2	24	0.14	0.2	208
1596	Ruiz	4	8100	40	1.0	11.4	0.04	0.1	90
1594	Raung	5	12,000	94	1.27	7.0	0.07	0.2	199

volcanic eruption. However, it is possible to speculate that two of them (1594 and 1596) might belong to the Raung (8°07′30″S 114°02′30″E) and Ruiz (04°53′43″N 75°19′21″W) volcanoes, whose eruptions were characterized by VEI values of 5 and 4 respectively.

Iron as a potential volcanic tracer has been proposed in previous studies. Spolaor et al. (Spolaor et al., 2012), detected a Fe^{2+} spike (up to 2 ng g^{-1}) 14 kyrs ago in the Talos Dome (Antarctica) ice core in correspondence with a sulphate peak (Severi et al., 2012). An increase in both soluble iron and soluble aluminium was recorded in coincidence with a volcanic eruption in another Greenland ice core (Spolaor et al., 2013b).

4.2. Iron speciation during volcanic eruptions

For the first time we provide a complete continuous iron speciation record of the B17 ice core in order to understand how the iron species were affected by volcanic eruptions.

The mean value for Fe^{2+} in quiescent time periods was 7 ± 4 pg g^{-1}, while in parallel to volcanic events, its value rose up to 560 pg g^{-1} (e.g. Huaynaputina). In general, we found that the Fe^{2+} concentration during volcanic eruptions was up to 2 orders of magnitude higher than the average value. This behaviour is confirmed for all the investigated volcanic eruptions suggesting that Fe^{2+} is a reliable volcanic eruption proxy.

Similarly, we observed that the total soluble iron increased during volcanic eruptions from an average value of 0.6 ± 0.2 ng g^{-1} up to 4 ng g^{-1} during the Huaynaputina eruption. However, the magnification of the signal was not as evident as for Fe^{2+}. Only for the Huaynaputina, Laki and Tambora eruptions we observed a significant increase in total soluble iron concentration, while, from 1820 to 1830 and from 1840 to 1850, we observed some spikes higher than 1 ng g^{-1} that are not associated with any volcanic eruptions. From this, we can conclude that soluble iron does not unambiguously indicate volcanic eruptions.

The same conclusion can be drawn for the total iron detected by the ICP-TOF-MS. We did not observe any significant increase in total iron concentration in coincidence with volcanic eruptions (excluding the Huaynaputina event). This suggests that it is impossible to discern the possible volcanic contribution from the seasonal contribution. The only spikes (up to 24 ng g^{-1}) that coincide with a volcanic eruption are those ones related to the Huaynaputina eruption.

4.3. Seasonality

Both total soluble iron and total iron exhibits a winter/spring seasonal pattern with values that ranged from below the LoD (0.020 ng g^{-1}) up to 2.0 ng g^{-1} and from below the LoD (0.043 ng g^{-1}) to 10 ng g^{-1} respectively. The soluble fraction, mainly constituted of Fe(III) species, represents $15 \pm 5\%$ of the total. The seasonality of the signal is caused by seasonally enhanced dust export mainly from Central Asian desert areas (Bory et al., 2002) with minor contributions potentially from the Sahara and Alaska (Lupker et al., 2010).

5. Conclusions

Iron is a key-element in different biogeochemical cycles playing a crucial role in regulating primary productivity in the HNLC regions. Through the validation of a new CFA-CL-Fe^{2+} method and the optimization of the existing total soluble iron method, we demonstrate the feasibility of Fe^{2+} quantification in ice cores, and that this also represents an excellent tool for detecting volcanic events and to date and synchronize ice cores. Indeed, through the correspondence between the Fe^{2+} peaks and the conductivity and sulphate peaks, we were able to identify up to 7 past volcanic events. Furthermore, the new CFA-CL-Fe^{2+} method is characterized by a low detection limit, high sensitivity, high accuracy, and good precision. All these features indicate that this technique might be particularly suitable for deep ice cores analyses where the low sample availability requires high-resolution techniques (for example for the EPICA Oldest Ice ice core project whose aim is to reconstruct the Earth climate and environmental conditions of the last 1.5 million years). While we could show that the occurrence of Fe^{2+} peaks in the B17 ice core can be clearly attributed to volcanic eruptions, the question is still open whether the higher Fe^{2+} levels are due to higher co-emission of Fe^{2+} and sulphate during the eruption or whether the higher pH in airborne aerosol in the volcanic plume leads to more Fe^{2+} leaching from total Fe. Moreover, future extended ice core studies should tackle the question whether Fe^{2+} deposition in ice cores is also a good proxy for total volcanic sulphur emission of an eruption, hence its radiative forcing in the stratosphere.

With the continuous total iron determination using the ICP-TOF-MS, we provide for the first time the complete iron speciation of an ice core by distinguishing the soluble Fe^{2+} and Fe^{3+} fractions as well as the particulate fraction of iron associated with aerosol. This work represents the first step to addressing the chemical iron speciation in ice cores. However, further studies through a multiproxy approach are needed to address this challenging paleo-environmental question.

Acknowledgments

For this work, I would like to thank prof. Paul Hansard (Department of Chemistry and Geochemistry, Colorado School of Mines, Golden, CO, USA) for the precious information he gave me about the luminol method and Mathias Bigler (formerly at University of Bern) for sharing his PhD thesis with me in order to deepen my knowledge about the continuous sulphate determination. Dr. Warren Cairns (Institute for the Dynamics of Environmental Processes) for suggestions and English revision. The division of Climate and Environmental Physics, Physics Institute, University of Bern gratefully acknowledges long-term financial support by the Swiss National Science Foundation (SNF).

Notes

The authors declare no competing financial interest.

Appendix A. Supplementary data

Supplementary data to this article can be found online at https://doi.org/10.1016/j.scitotenv.2018.11.075.

References

Achterberg, E.P., Holland, T.W., Bowie, A.R., Mantoura, R.F.C., Worsfold, P.J., 2001. Determination of iron in seawater. Anal. Chim. Acta 442, 1–14.

Barbante, C., Bellomi, T., Mezzadri, G., Cescon, P., Scarponi, G., Morel, C., et al., 1997. Direct determination of heavy metals at picogram per gram levels in Greenland and Antarctic snow by double focusing inductively coupled plasma mass spectrometry. J. Anal. At. Spectrom. 12, 925–931.

Bigler, M., Wagenbach, D., Fischer, H., Kipfstuhl, J., Miller, H., Sommer, S., et al., 2002. Sulphate record from a northeast Greenland ice core over the last 1200 years based on continuous flow analysis. Ann. Glaciol. 35, 250–256.

Bory, A.-M., Biscaye, P.E., Svensson, A., Grousset, F.E., 2002. Seasonal variability in the origin of recent atmospheric mineral dust at NorthGRIP, Greenland. Earth Planet. Sci. Lett. 196, 123–134.

Chan, K., Jiang, S., Ning, Z., 2016. Speciation of water soluble iron in size segregated airborne particulate matter using LED based liquid waveguide with a novel dispersive absorption spectroscopic measurement technique. Anal. Chim. Acta 914, 100–109.

Collins, R.N., Kinsela, A.S., 2010. The aqueous phase speciation and chemistry of cobalt in terrestrial environments. Chemosphere 79, 763–771.

Croot, P.L., Laan, P., 2002. Continuous shipboard determination of Fe (II) in polar waters using flow injection analysis with chemiluminescence detection. Anal. Chim. Acta 466, 261–273.

Dai, J., Mosley-Thompson, E., Thompson, L.G., 1991. Ice core evidence for an explosive tropical volcanic eruption 6 years preceding Tambora. J. Geophys. Res.-Atmos. 96, 17361–17366.

D'Arrigo, R., Wilson, R., Tudhope, A., 2009. The impact of volcanic forcing on tropical temperatures during the past four centuries. Nat. Geosci. 2, 51.

Emmenegger, L., King, D.W., Sigg, L., Sulzberger, B., 1998. Oxidation kinetics of Fe (II) in a eutrophic Swiss lake. Environ. Sci. Technol. 32, 2990–2996.

Gautier, E., Savarino, J., Erbland, J., Lanciki, A., Possenti, P., 2015. Variability of sulfate signal in ice-core records based on five replicate cores. Clim. Past Discuss. 11, 3973–4002.

González, A.G., Pérez-Almeida, N., Magdalena Santana-Casiano, J., Millero, F.J., González-Dávila, M., 2016. Redox interactions of Fe and Cu in seawater. Mar. Chem. 179, 12–22.

Hansard, S.P., Landing, W.M., 2009. Determination of iron (II) in acidified seawater samples by luminol chemiluminescence. Limnol. Oceanogr. Methods 7, 222–234.

Hendriks, L., Gundlach-Graham, A., Hattendorf, B., Günther, D., 2017. Characterization of a new ICP-TOFMS instrument with continuous and discrete introduction of solutions. J. Anal. At. Spectrom. 32, 548–561.

Hirayama, K., Unohara, N., 1988. Spectrophotometric catalytic determination of an ultratrace amount of iron (III) in water based on the oxidation of *N*,*N*-dimethyl-*p*-phenylenediamine by hydrogen peroxide. Anal. Chem. 60, 2573–2577.

Hiscock, W.T., Fischer, H., Bigler, M., Gfeller, G., Leuenberger, D., Mini, O., 2013. Continuous flow analysis of labile iron in ice-cores. Environ. Sci. Technol. 47, 4416–4425.

Huybers, P., Langmuir, C., 2009. Feedback between deglaciation, volcanism, and atmospheric CO_2. Earth Planet. Sci. Lett. 286, 479–491.

Kaufmann, P.R., Federer, U., Hutterli, M.A., Bigler, M., Schüpbach, S., Ruth, U., et al., 2008. An improved continuous flow analysis system for high-resolution field measurements on ice cores. Environ. Sci. Technol. 42, 8044–8050.

King, D.W., Lounsbury, H.A., Millero, F.J., 1995. Rates and mechanism of Fe (II) oxidation at nanomolar total iron concentrations. Environ. Sci. Technol. 29, 818–824.

Kjær, H.A., Vallelonga, P., Svensson, A., Elleskov, L., Kristensen, M., Tibuleac, C., Winstrup, M., et al., 2016. An optical dye method for continuous determination of acidity in ice cores. Environ. Sci. Technol. 50, 10485–10493.

Knüsel, S., Piguet, D.E., Schwikowski, M., Gäggeler, H.W., 2003. Accuracy of continuous ice-core trace-element analysis by inductively coupled plasma sector field mass spectrometry. Environ. Sci. Technol. 37, 2267–2273.

Langmann, B., Zakšek, K., Hort, M., Duggen, S., 2010. Volcanic ash as fertiliser for the surface ocean. Atmos. Chem. Phys. 10, 3891–3899.

Lannuzel, D., De Jong, J., Schoemann, V., Trevena, A., Tison, J.-L., Chou, L., 2006. Development of a sampling and flow injection analysis technique for iron determination in the sea ice environment. Anal. Chim. Acta 556, 476–483.

Longpré, M.A., Stix, J., Burkert, C., Hansteen, T., Kutterolf, S., 2014. Sulfur budget and global climate impact of the AD 1835 eruption of Cosigüina volcano, Nicaragua. Geophys. Res. Lett. 41, 6667–6675.

Lupker, M., Aciego, S.M., Bourdon, B., Schwander, J., Stocker, T., 2010. Isotopic tracing (Sr, Nd, U and Hf) of continental and marine aerosols in an 18th century section of the Dye-3 ice core (Greenland). Earth Planet. Sci. Lett. 295, 277–286.

Madsen, B.C., Murphy, R.J., 1981. Flow injection and photometric determination of sulfate in rainwater with methylthymol blue. Anal. Chem. 53, 1924–1926.

Majestic, B.J., Schauer, J.J., Shafer, M.M., Turner, J.R., Fine, P.M., Singh, M., et al., 2006. Development of a wet-chemical method for the speciation of iron in atmospheric aerosols. Environ. Sci. Technol. 40, 2346–2351.

Martin, J.H., Fitzwater, S.E., 1988. Iron deficiency limits phytoplankton growth in the north-east Pacific subarctic. Nature 331, 341.

Martin, J.H., Gordon, R.M., Fitzwater, S.E., 1990. Iron in Antarctic waters. Nature 345, 156.

McConnell, J.R., Lamorey, G.W., Lambert, S.W., Taylor, K.C., 2002. Continuous ice-core chemical analyses using inductively coupled plasma mass spectrometry. Environ. Sci. Technol. 36, 7–11.

Morgan, B., Lahav, O., 2007. The effect of pH on the kinetics of spontaneous Fe (II) oxidation by O_2 in aqueous solution–basic principles and a simple heuristic description. Chemosphere 68, 2080–2084.

Newhall, C.G., Self, S., 1982. The volcanic explosivity index (VEI) an estimate of explosive magnitude for historical volcanism. J. Geophys. Res. Oceans 87, 1231–1238.

Oppenheimer, C., 2003. Climatic, environmental and human consequences of the largest known historic eruption: Tambora volcano (Indonesia) 1815. Prog. Phys. Geogr. Earth Environ. 27, 230–259.

Pullin, M.J., Cabaniss, S.E., 2001. Colorimetric flow-injection analysis of dissolved iron in high DOC waters. Water Res. 35, 363–372.

Raible, C.C., Brönnimann, S., Auchmann, R., Brohan, P., Frölicher, T.L., Graf, H.F., et al., 2016. Tambora 1815 as a test case for high impact volcanic eruptions: earth system effects. Wiley Interdiscip. Rev. Clim. Chang. 7, 569–589.

Rose, A.L., Waite, T.D., 2001. Chemiluminescence of luminol in the presence of iron (II) and oxygen: oxidation mechanism and implications for its analytical use. Anal. Chem. 73, 5909–5920.

Röthlisberger, R., Bigler, M., Hutterli, M., Sommer, S., Stauffer, B., Junghans, H.G., et al., 2000. Technique for continuous high-resolution analysis of trace substances in firn and ice cores. Environ. Sci. Technol. 34, 338–342.

Saitoh, K., Hasebe, T., Teshima, N., Kurihara, M., Kawashima, T., 1998. Simultaneous flow-injection determination of iron (II) and total iron by micelle enhanced luminol chemiluminescence. Anal. Chim. Acta 376, 247–254.

Santana-González, C., Santana-Casiano, J.M., González-Dávila, M., Fraile-Nuez, E., 2017. Emissions of Fe (II) and its kinetic of oxidation at Tagoro submarine volcano, El Hierro. Mar. Chem. 195, 129–137.

Schallenberg, C., van der Merwe, P., Chever, F., Cullen, J.T., Lannuzel, D., Bowie, A.R., 2016. Dissolved iron and iron (II) distributions beneath the pack ice in the East Antarctic (120 E) during the winter/spring transition. Deep-Sea Res. II Top. Stud. Oceanogr. 131, 96–110.

Scott, W., Gardner, C., Devoli, G., Alvarez, A., 2006. The A. D. 1835 eruption of Volcán Cosigüina, Nicaragua: a guide for assessing local volcanic hazards. Volcanic Hazards Cent. Am. 412, 167.

Seitz, W.R., Hercules, D.M., 1972. Determination of trace amounts of iron (II) using chemiluminescence analysis. Anal. Chem. 44, 2143–2149.

Severi, M., Udisti, R., Becagli, S., Stenni, B., Traversi, R., 2012. Volcanic synchronisation of the EPICA-DC and TALDICE ice cores for the last 42 kyr BP. Clim. Past 8, 509–517.

Severi, M., Becagli, S., Traversi, R., Udisti, R., 2015. Recovering paleo-records from Antarctic ice-cores by coupling a continuous melting device and fast ion chromatography. Anal. Chem. 87, 11441–11447.

Sigl, M., McConnell, J.R., Layman, L., Maselli, O., McGwire, K., Pasteris, D., et al., 2013. A new bipolar ice core record of volcanism from WAIS Divide and NEEM and implications for climate forcing of the last 2000 years. J. Geophys. Res.-Atmos. 118, 1151–1169.

Sigl, M., McConnell, J.R., Toohey, M., Curran, M., Das, S.B., Edwards, R., et al., 2014. Insights from Antarctica on volcanic forcing during the Common Era. Nat. Clim. Chang. 4, 693.

Sigl, M., Winstrup, M., McConnell, J., Welten, K., Plunkett, G., Ludlow, F., et al., 2015. Timing and climate forcing of volcanic eruptions for the past 2,500 years. Nature 523, 543.

Spirakis, C.S., 1991. Iron fertilization with volcanic ash? Eos. Trans. AGU 72, 525-525.

Spolaor, A., Vallelonga, P., Gabrieli, J., Cozzi, G., Boutron, C., Barbante, C., 2012. Determination of Fe^{2+} and Fe^{3+} species by FIA-CRC-ICP-MS in Antarctic ice samples. J. Anal. At. Spectrom. 27, 310–317.

Spolaor, A., Vallelonga, P., Cozzi, G., Gabrieli, J., Varin, C., Kehrwald, N., et al., 2013a. Iron speciation in aerosol dust influences iron bioavailability over glacial-interglacial timescales. Geophys. Res. Lett. 40, 1618–1623.

Spolaor, A., Vallelonga, P., Gabrieli, J., Roman, M., Barbante, C., 2013b. Continuous flow analysis method for determination of soluble iron and aluminium in ice cores. Anal. Bioanal. Chem. 405, 767–774.

Stookey, L.L., 1970. Ferrozine—a new spectrophotometric reagent for iron. Anal. Chem. 42, 779–781.

Thordarson, T., Self, S., 2003. Atmospheric and environmental effects of the 1783–1784 Laki eruption: a review and reassessment. J. Geophys. Res.-Atmos. 108.

Traversi, R., Barbante, C., Gaspari, V., Fattori, I., Largiuni, O., Magaldi, L., et al., 2004. Aluminium and iron record for the last 28 kyr derived from the Antarctic EDC96 ice core using new CFA methods. Ann. Glaciol. 39, 300–306.

Vinther, B.M., Clausen, H.B., Johnsen, S.J., Rasmussen, S.O., Andersen, K.K., Buchardt, S.L., et al., 2006. A synchronized dating of three Greenland ice cores throughout the Holocene. J. Geophys. Res.-Atmos. 111.

Watson, A.J., 1997. Volcanic iron, CO_2, ocean productivity and climate. Nature 385, 587.

Weissbach, S., Wegner, A., Opel, T., Oerter, H., Vinther, B., Kipfstuhl, S., 2016. Spatial and temporal oxygen isotope variability in northern Greenland–implications for a new climate record over the past millennium. Clim. Past 12, 171–188.

Williams, M., 2012. The ~73 ka Toba super-eruption and its impact: history of a debate. Quat. Int. 258, 19–29.

Yalcin, K., Wake, C.P., Kreutz, K.J., Germani, M.S., Whitlow, S.I., 2006. Ice core evidence for a second volcanic eruption around 1809 in the Northern Hemisphere. Geophys. Res. Lett. 33.

Yuan, J., Resing, J., 1995. Determination of iron in seawater by flow injection analysis using in-line preconcentration and spectrophotometric detection. Mar. Chem. 50, 3–12.

Zhuang, G., Yi, Z., Wallace, G.T., 1995. Iron (II) in rainwater, snow, and surface seawater from a coastal environment. Mar. Chem. 50, 41–50.

Zielinski, G.A., 2000. Use of paleo-records in determining variability within the volcanism–climate system. Quat. Sci. Rev. 19, 417–438.